Human cytomegalovirus pUL37x1-induced calcium flux activates PKCα, inducing altered cell shape and accumulation of cytoplasmic vesicles

Ronit Sharon-Friling and Thomas Shenk[1]

Department of Molecular Biology, Princeton University, Princeton, NJ 08544

Contributed by Thomas Shenk, February 11, 2014 (sent for review December 27, 2013)

The human cytomegalovirus immediate-early protein pUL37x1 induces the release of Ca^{2+} stores from the endoplasmic reticulum into the cytosol. This release causes reorganization of the cellular actin cytoskeleton with concomitant cell rounding. Here we demonstrate that pUL37x1 activates Ca^{2+}-dependent protein kinase Cα (PKCα). Both PKCα and Rho-associated protein kinases are required for actin reorganization and cell rounding; however, only PKCα is required for the efficient production of virus progeny, arguing that HCMV depends on the kinase for a second function. PKCα activation is also needed for the production of large (1–5 μm) cytoplasmic vesicles late after infection. The production of these vesicles is blocked by inhibition of fatty acid or phosphatidylinositol-3-phosphate biosynthesis, and the failure to produce vesicles is correlated with substantially reduced production of enveloped virus capsids. These results connect earlier work identifying a requirement for lipid synthesis with specific morphological changes, and support the argument that the PKCα-induced large vesicles are either required for the efficient production of mature virus particles or serve as a marker for the process.

capsid envelopment | virion assembly | virus-induced membranes

Human cytomegalovirus (HCMV), a ubiquitous β-herpesvirus, is a major cause of birth defects and an opportunistic agent in immunosuppressed individuals (1). In addition, it has been associated with glioblastoma and other cancers (2), cardiovascular disease (3), and immune sensescence (4). Cytomegalovirus is named for the morphological changes —enlarged cells with nuclear and cytoplasmic inclusions—observed in cytomegalic inclusion disease (5). Striking morphological changes have been documented after infection of cultured fibroblasts with HCMV, including cell rounding, enlarged nuclei with a distorted kidney-like shape, and production of a membranous structure adjacent to the concave surface of the nucleus known as the assembly compartment (6–8).

Cell rounding is induced by the viral immediate-early protein, pUL37x1 (9, 10). This membrane-associated protein accumulates in the endoplasmic reticulum and mitochondria (11). pUL37x1 blocks apoptosis, and thus is also known as the viral mitochondria-localized inhibitor of apoptosis (12). Cell rounding results from pUL37x1-induced release of Ca^{2+} from the endoplasmic reticulum into the cytosol, causing reorganization of the actin cytoskeleton (10).

In the present study, we identified a cellular signaling pathway activated by pUL37x1. Ca^{2+} mobilization was found to induce activation of protein kinase Cα (PKCα), which is required for cell rounding and the efficient production of progeny virus. PKCα-dependent cell rounding was substantially blocked by Rho-associated protein kinase (ROCK) inhibitors, implicating Rho GTPases in the morphological change; however, inhibition of rounding did not reduce HCMV yield. Inhibition of PKCα had a second effect on the morphology of infected cells, blocking the production of large cytoplasmic vesicles that accumulate during the late phase of infection. Accumulation of these vesicles required two enzymes that support lipid synthesis, acetyl-CoA carboxylase and class III phosphatidylinsoitol 3-kinase (Vps34). Inhibition of either enzyme not only blocked production of the vesicles, but also reduced the yield of infectious progeny.

Results

HCMV pUL37x1 Induces Dynamic Changes in Cell Shape. During infection of fibroblasts with HCMV, the earliest visible cytopathic effect is a change in cell shape caused by pUL37x1 (9, 10). This viral protein mobilizes Ca^{2+} from the endoplasmic reticulum into the cytosol, which induces reorganization of the actin cytoskeleton and cell rounding. To confirm and quantify the effect of pUL37x1 on cell shape, we used a cell-permeable fluorophore, calcein AM, to monitor the shape of infected cells on confocal microscopy. At 24 h after mock infection (Fig. 1*A*, *Upper*, mock), cells exhibited an elongated and flattened morphology. When these cells were infected with WT HCMV, they transformed from long and thin to rounded at 24 h postinfection (hpi) (Fig. 1*A*, *Upper*, 24 hpi). Although individual cells varied, on average infected cells displayed a 5.9-fold increase in height (*z*-axis) relative to mock-infected counterparts ($P < 0.001$) (Fig. 1*B, Upper*). At 72 hpi, the cells became less spherical, assuming a hemispherical shape, with a 4.7-fold increase in the *z*-axis relative to mock-infected ($P < 0.001$). Treatment with a cell-permeable calcium chelator, BAPTA-AM, prevented the changes induced by infection (Fig. 1*A*, *Upper*, +BAPTA).

To verify that the changes in cell morphology are related specifically to pUL37x1, we expressed this protein in uninfected fibroblasts. This induced the spherical shape, and treatment with BAPTA-AM prevented the change (Fig. 1*A, Lower*, pUL37x1). Conversely, a mutant virus (BAD*sub*UL37x1) unable to express pUL37x1, and thus unable to induce Ca^{2+} flux to the cytosol (10), produced only modest changes in shape (1.3- and 1.6-fold increase in the *z*-axis relative to mock-infected at 24 and 72 hpi, respectively) (Fig. 1*A*, *Lower*, BAD*sub*UL37x1; Fig. 1*B, Lower*,

Significance

The human cytomegalovirus protein, pUL37x1, induces the release of calcium from the endoplasmic reticulum into the cytosol, causing reorganization of the infected cell's actin network with concomitant cell rounding. This study demonstrates that along with its effects on cell shape, calcium release induces the formation of large cytoplasmic vesicles late after infection. This formation requires the activity of a calcium-dependent kinase, protein kinase Cα, as well as enzymes required for the synthesis of fatty acids and lipids. The failure to produce vesicles is correlated with the reduced production of infectious, enveloped virus particles. This work identifies an additional consequence of pUL37x1 action and links de novo lipid synthesis with a specific morphological change after infection.

Author contributions: R.S.-F. and T.S. designed research; R.S.-F. performed research; R.S.-F. and T.S. analyzed data; and R.S.-F. and T.S. wrote the paper.

The authors declare no conflict of interest.

[1]To whom correspondence should be addressed. E-mail: tshenk@princeton.edu.

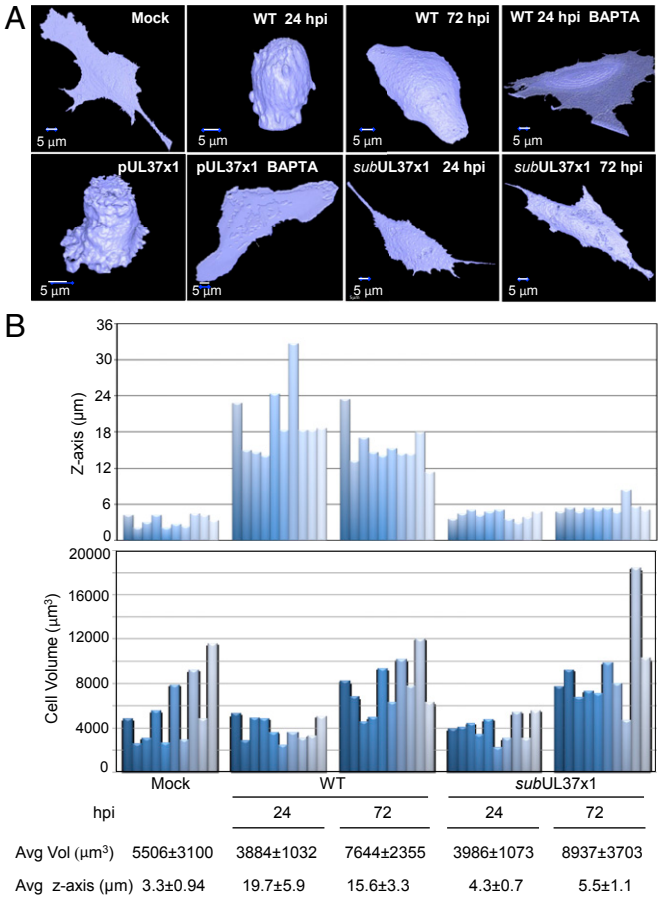

Fig. 1. Morphological changes induced by pUL37x1. (*A*) pUL37x1 induces calcium-dependent shape changes after infection. Fibroblasts were mock-infected or infected with WT or pUL37x1-deficient (*sub*UL37x1) HCMV. Alternatively, cultures (5×10^6 cells) were electroporated with 5 μg of a pUL37x1 expression plasmid in the absence of infection. Cells were analyzed at 24 and 72 hpi or at 24 h after electrophoration by treatment with 5 μM fluorophore calcein AM for 1 h, followed by spinning disk confocal Z-stack live cell imaging and reconstruction of 3D images. Where indicated, cells were pretreated with 10 μM BAPTA-AM for 1 h before infection or transfection. (*B*) Quantification of infected cell height and volume. (*Upper*) Height and volume measurements of 10 individual cells selected from mock-infected, WT-infected, and subUL37x1-infected fibroblasts treated with calcein AM. (*Lower*) Average (Avg) height from the surface of the plate (*z*-axis) and volume (Vol).

average *z*-axis). Whereas WT virus infection or pUL37x1 expression alone caused a marked topological change in all cells, the total cell volume was variable when individual cells were measured (Fig. 1*B, Lower*). This variation was expected, because subconfluent cells at different stages of the cell cycle were infected to allow precise delineation of cell boundaries for shape determination. These experiments confirm that the previously identified cytoskeletal reorganization is accompanied by profound pUL37x1-dependent changes in cell shape.

HCMV pUL37x1 Activates PKCα. Given the role for Ca^{2+} in the topological changes (Fig. 1) and cytoskeletal reorganization (10) after infection, we hypothesized that the Ca^{2+}-dependent kinase PKCα might contribute to the process because it can modulate the actin cytoskeleton (13, 14). Cytosolic Ca^{2+} induces the translocation of Ca^{2+}-bound PKCα to the plasma membrane, where the kinase is activated although its interaction with diacylglycerol (15). To test whether HCMV induces the translocation of PKCα, we transfected fibroblasts with a plasmid expressing PKCα fused to GFP (16, 17), and then mock-infected or infected the cultures. Analysis of 2D optical sections by confocal microscopy revealed that a portion of PKCα-GFP was translocated from the cytoplasm to foci at the plasma membrane at 8–16 hpi with WT HCMV (Fig. 2, *Upper*, mock vs. WT), but not with BAD*sub*UL37x1 (Fig. 2, *Lower Center* and *Right*). Consistent with a role for pUL37x1-driven Ca^{2+} flux, BAPTA-AM inhibited PKCα translocation after infection with WT virus (Fig. 2, *Lower Left*).

Treatment with a PKCα-specific shRNA (Fig. 3*A*, *Right*) or antagonist (Gö6976) substantially blocked remodeling of the actin cytoskeleton and cell rounding at 24 hpi when assayed by actin staining (Fig. 3*A*, *Left*) or by observing cell shape (Fig. 3*B*). Consistent with an earlier report (18), WT virus also substantially reduced cell surface staining with vinculin (Fig. 3*A*, *Upper*), a protein found at the intersection of actin bundles and membrane attachment sites (19). Vinculin staining was not reduced by infection after treatment with PKCα-specific shRNA or drug. PKCα-specific shRNA delayed the production of progeny and reduced HCMV yield by a factor of nearly 100 (Fig. 3*C*), and Gö6976 reduced virus yield to a similar extent (Fig. 3*D*). Thus, PKCα activity is necessary for the morphological changes induced by pUL37x1 and for the timely and efficient production of progeny virus.

PKCα can activate the Rho GTPase, RhoA, by phosphorylating and inducing release of the rho guanine dissociation inhibitor (20). RhoA in turn can impact the actin cytoskeleton (21, 22) through multiple downstream effectors, including the Rho-associated protein kinases (ROCK1 and ROCK2) (23). Because pharmacologic inhibition of ROCKs can alter fibroblast shape (24, 25), we tested for a role of the kinases in the morphological changes induced by HCMV. We used two structurally unrelated antagonists at doses expected to inhibit both ROCKs (Y27632, 10 μM; GSK429286A, 140 nM). The drugs substantially blocked the cell rounding normally observed at 24 hpi with WT HCMV when assayed by actin staining (Fig. 4*A*) or by monitoring cell shape (Fig. 4*B*). The cells transitioned directly to the hemispherical shape characteristic of the late phase of infection. Although they altered the program of morphological changes, neither drug influenced the yield of HCMV (Fig. 4*C*). We conclude that the transient cell rounding evident at 24 hpi is not required for optimal virus replication in cultured fibroblasts.

Activated PKCα interacts with the primary caveolar protein, caveolin-1 (26, 27). Caveolin-1 is a major constituent of lipid

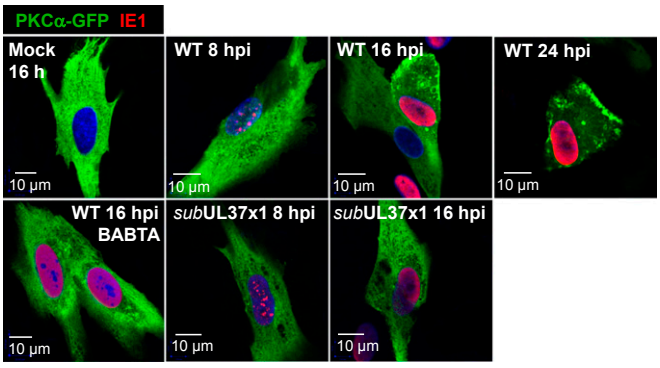

Fig. 2. Calcium-dependent transport of PKCα to the plasma membrane requires expression of pUL37x1. Fibroblasts were electroporated with 5 μg of PKCα-GFP expression plasmid, infected 24 h later with WT or *sub*UL37x1, and assayed for fluorescence (green) at the indicated times after infection. HCMV IE1 (red) was monitored to confirm infection, and DNA was stained with DAPI (blue). Where indicated, cells were pretreated with 10 μM BAPTA-AM for 1 h before infection or transfection.

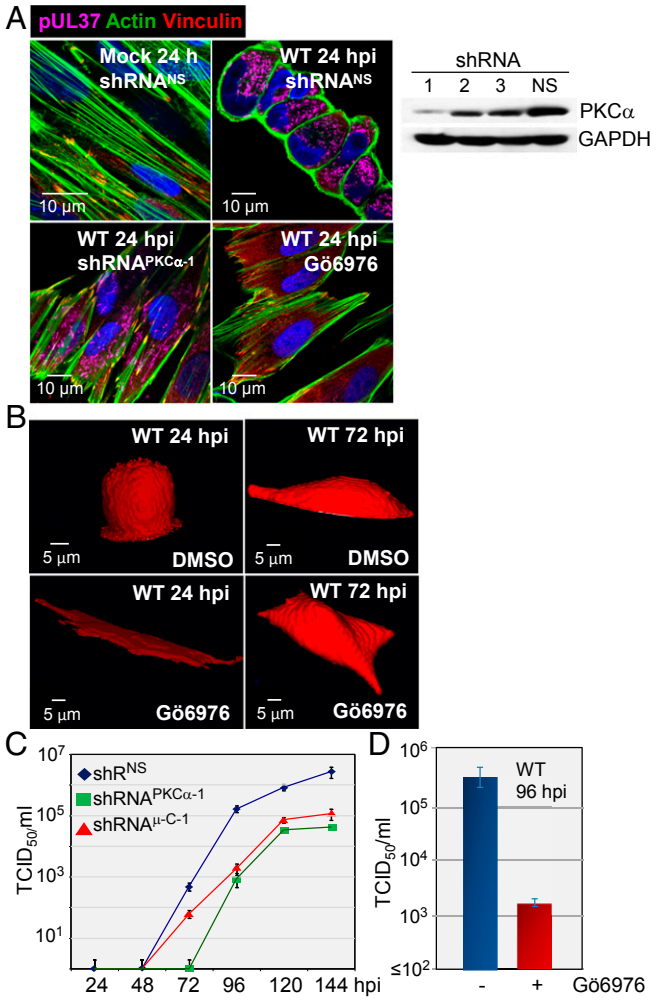

Fig. 3. PKCα is required for actin reorganization after infection. (*A*) shRNA-mediated knockdown of PKCα inhibits actin reorganization after infection. (*Right*) Fibroblasts were treated with PKCα-specific shRNAs (1–3) or a nonspecific shRNA (NS), and kinase levels were assayed 10 d later by Western blot analysis using antibody to PKCα. Cellular GAPDH was monitored as a loading control. (*Left*) shRNA-treated cells were mock-infected or infected with WT virus at a multiplicity of 3 pfu/cell. Treatment with 1 μM Gö6976, a PKCα-specific inhibitor, was initiated at 1 h after infection and continued until 24 hpi, when cultures were assayed for actin (green) and vinculin (red). pUL37 (purple) was monitored to confirm infection, and DNA was stained with DAPI (blue). (*B*) Reduced PKCα activity inhibits cell rounding at 24 hpi. Fibroblasts received solvent (DMSO) or 1 μM Gö6976 beginning 1 h after infection with WT or *sub*UL37x1 and analyzed by treatment with 5 μM fluorophore calcein red-orange AM for 1 h, followed by spinning disk confocal Z-stack live cell imaging and reconstruction of 3D images. Cultures received fresh medium plus drug every 24 h. (*C*) PKCα and μ-calpain (μC-1) are required for optimal HCMV yield. Fibroblasts treated with a nonspecific shRNA (black diamonds) or PKCα-specific shRNA (green squares) or μ-calpain (red triangles) were infected with WT HCMV, and extracellular virus was quantified by a $TDIC_{50}$ assay. (*D*) Virus production was assayed by $TDIC_{50}$ at 96 hpi in cultures treated with 1 μM Gö6976.

rafts (28, 29), which serve as dynamic signaling scaffolds (30) and whose spatial distribution in the plasma membrane is driven in part by proteins linked to the underlying cortical actin cytoskeleton (31, 32). Given the PKCα-dependent perturbation of the cytoskeleton during infection (Fig. 3*B*) and its association with caveolin, we tested the possibility that on infection, the kinase might translocate to lipid rafts, whose proteins are experimentally defined as detergent-resistant membrane (DRM) proteins. Fibroblast membranes were solubilized with Triton X-100, and DRM proteins were identified by flotation in sucrose gradients. A portion of the PKCα floated near the top of the gradient, coincident with the DRM marker ganglioside GM1 at 24 and 72 hpi with WT HCMV (Fig. 5*A*, *Upper*, fractions 8 and 9). In contrast, PKCα from extracts of mock-infected or BAD*sub*UL37 virus-infected cells traveled with the detergent-soluble fraction, as demonstrated by its coincidence with the transferrin receptor (Fig. 5*A*, *Lower*, fractions 2–7).

At 72 hpi, a 45-kDa polypeptide that reacted with PKCα-specific antibody was present in the DRM fraction in place of the full-length 80-kDa protein (Fig. 5*A*, *Upper Right*, fractions 7–9). Previous studies have shown that μ-calpain, a Ca^{2+}-activated protease, can cleave PKCα to produce a 45-kDa catalytic fragment and a 36-kDa regulatory fragment (28, 33). When μ-calpain was knocked down by shRNA treatment (Fig. 5*B*, *Left*), the amount of the 45-kDa species in total cell extracts was reduced at 72 hpi (Fig. 5*B*, *Right*), suggesting that the protease is responsible for PKCα cleavage during infection. All of the PKCα in the DRM fraction was cleaved (Fig. 5*A*, *Upper Right*, lanes 7–9), whereas only a portion of the total PKCα was cleaved (Fig. 5*A*, *Upper Right* and Fig. 5*B*), indicating that μ-calpain acts at the membrane. Knockdown of μ-calpain also decreased virus yield (Fig. 3*C*), indicating that cleavage of PKCα or another target of the protease is required for optimal virus production. A 45-kDa fragment produced by μ-calpain cleavage has been reported to exhibit constitutive PKCα activity (14, 34), raising the possibility

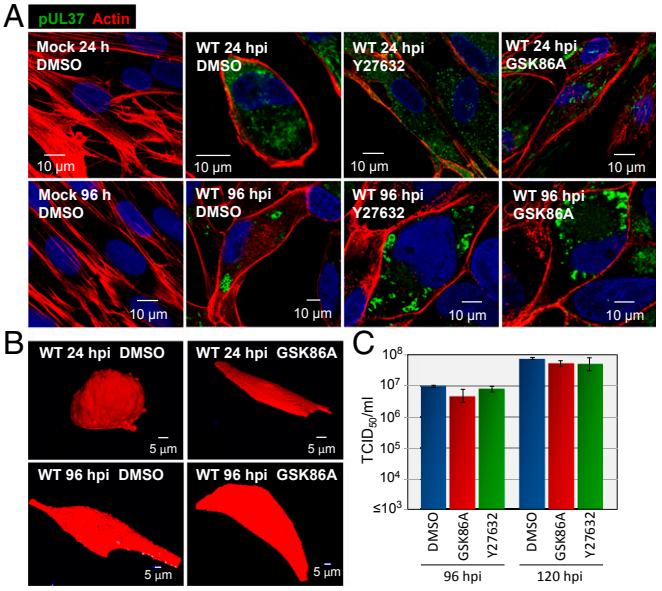

Fig. 4. ROCK antagonists interfere with infection-induced changes in cell shape, but do not reduce HCMV yield. (*A*) ROCK antagonists block actin reorganization after infection. Fibroblasts were treated with solvent (DMSO) or drug (10 μM Y27632 or 140 nM GSK429286A) beginning 1 h after mock infection or infection with WT virus. Cells received fresh medium containing solvent or drug every 24 h. Cultures were assayed for actin using labeled phalloidin (red), pUL37 (green), and DNA (blue). (*B*) ROCK antagonist blocks cell rounding at 24 hpi. Fibroblasts were treated with solvent or drug beginning 1 h after mock infection or infection with WT virus. Cultures received fresh medium with drug every 24 h and were analyzed by treatment with 5 μM fluorophore calcein red-orange AM for 1 h, followed by spinning disk confocal Z-stack live cell imaging and reconstruction of 3D images. (*C*) ROCK activity does not influence virus yield. Fibroblasts were treated with solvent or ROCK antagonists beginning 1 h after infection with WT HCMV. Cultures received fresh medium with drug every 24 h, and extracellular virus yields were determined by plaque assay.

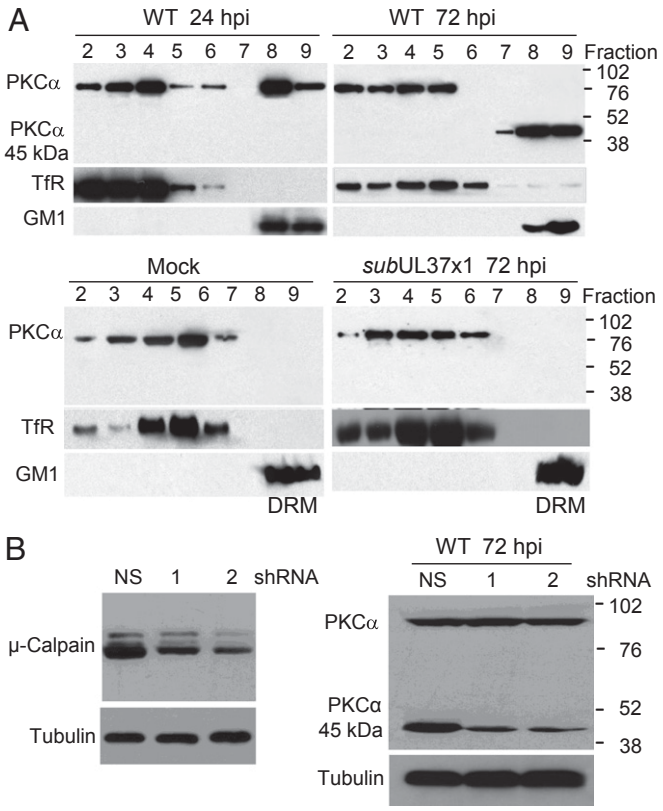

Fig. 5. PKCα is enriched in lipid raft/DRM fractions after infection with WT, but not with pUL37x1-deficient, HCMV. (*A*) PKCα moves to the DRM fraction after infection. Fibroblasts were mock-infected or infected with WT or *sub*UL37x1. At indicated times, cells were lysed and subjected to centrifugation in Optiprep gradients, and fractions (fraction 9, top of gradient) were assayed by Western blot analysis for PKCα. Markers for the DRM fraction [ganglioside (GM1)] and soluble membrane fraction [transferrin receptor (TfR)] were assayed as controls. (*B*) μ-calpain cleaves PKCα after infection. (*Left*) Cells were treated with nonspecific (NS) or μ-calpain–specific shRNAs (1 and 2) and assayed 10 d later by Western blot analysis using μ-calpain–specific antibody. Tubulin was assayed as a loading control. (*Right*) Fibroblasts treated with nonspecific or μ-calpain–specific shRNAs were assayed for PKCα by Western blot analysis, with tubulin assayed as a control.

that over time, infection may uncouple PKCα from its normal dependence on Ca^{2+} and lipids.

HCMV pUL37x1 Induces PKCα-Dependent Accumulation of Large Cytoplasmic Vesicles. The cytoplasmic virion assembly compartment (AC) is an HCMV-induced membranous structure formed proximal to the concave surface of the infected cell nucleus (6–8). The AC is thought to be where virions acquire tegument proteins and envelopes. Early endosome antigen-1 (EEA1) is a cellular protein present in early endosomes (35) that participates in endosomal membrane fusion (36) and is localized to the AC within infected cells (37, 38). Our findings confirm these characteristics, showing that EEA1 was colocalized with two markers of the AC, a Golgi component targeted by HPA lectin and the late viral protein pUL99 (Fig. 6*A*, *Upper*). EEA1 and pUL99 also localized at the periphery of large vesicles. Similar vesicles have been described previously (7, 39). EEA1 binds to the head group of phosphatidylinositol-3-phosphate (PtdIns3*P*) (35, 40), and pUL99 associates with membranes through its myristoyl modification (41), so it is likely that the two proteins associate with the large vesicles at their membranes. The vesicles ranged in size from approximately 0.5 μM to nearly 5.0 μM in diameter (Fig. 6*B*, *Upper Left*), and they were also evident on examination of cells by differential interference contrast (DIC) microscopy (Fig. 6*B*, *Upper Right*). Although EEA1 and pUL99 appeared in the AC after infection with BAD*sub*UL37x1, no large vesicles with pUL99 were generated (Fig. 6*A*, *Lower*). Furthermore, no large vesicles were detected in mutant virus-infected cells by DIC microscopy (Fig. 6*B*, *Lower Right*), ruling out the possibility that the vesicles accumulated but did not associate with the viral protein.

It was recently reported that siRNA-mediated knockdown of EEA1 modulates the activation of PKCα (42). Given our results showing a role for PKCα in the production of infectious virus (Fig. 3*C*), we surmised that a PKCα-EEA1 functional connection might be relevant to HCMV replication. We initially tested the possibility that, like PKCα, EEA1 might associate with lipid rafts after infection. EEA1 was present in the DRM fraction of WT-infected cells, but not in that of mock-infected or BAD*sub*UL37-infected cells (Fig. 6*C*). Whereas only full-length (180 kDa) EEA1 protein was detected in mock-infected or BAD*sub*UL37x1-infected cells, both full-length protein and three more rapidly migrating bands (~70, 50, and 40 kDa) reacted with the EEA1-specific

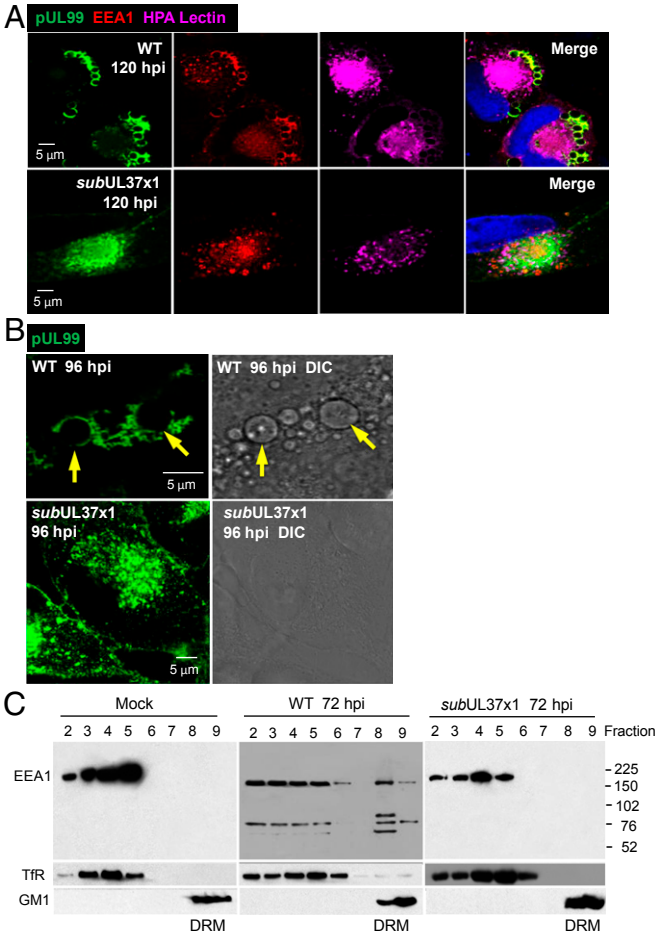

Fig. 6. Large vesicles containing pUL99 and EEA1 accumulate in the cytoplasm of WT-infected, but not *sub*UL37x1-infected, cells. (*A*) pUL37x1-expressing virus induces accumulation of large cytoplasmic vesicles. Infected cells were assayed by immunofluorescence at 120 hpi for pUL99 (green), EEA1 (red), or the Golgi tag HPA lectin (purple). (*B*) Large pUL99-containing vesicles are revealed by DIC microscopy at 96 hpi with WT, but not with *sub*UL37x1. Arrows indicate vesicles in identical immunofluorescent and DIC images. (*C*) EEA1 moves to the DRM fraction after infection. Cells were treated and lysates processed as described for Fig. 5, and then assayed by Western blot analysis for EEA1 and marker proteins.

antibody in the DRM fraction of WT virus-infected cells. The origin and functional significance of these fragments are unknown; nevertheless, we can conclude that PKCα and EEA1 cosediment with the DRM fraction in response to the action of pUL37x1.

Because EEA1 normally localizes to the early endosome membrane (35), its association with the large pUL99-positive vesicles suggests that they might be functional early endosomes. To test this possibility, we monitored the uptake of Alexa Fluor 594-labeled dextran from the medium, an assay in which the dextran accumulates in early endosomes (43). The pUL99-positive vesicles were again readily identified by DIC imaging (Fig. 7, yellow arrows). Although small vesicles internalizing labeled dextran were clearly visible, there was no evidence of dextran uptake into the large vesicles at 96 or 120 hpi (Fig. 7, *Top* and *Middle*). Furthermore, shRNA-mediated knockdown of Vps34 showed no diminution of the Alexa Fluor 594 signal in the small vesicles (Fig. 7, bottom panels), in agreement with previous observations (44). These results suggest that the large vesicles are not functional early endosomes.

Given the colocalization of PKCα and EEA1 in the DRM fraction of infected cells, we tested the possibility that PKCα is required for accumulation of the large vesicles. Treatment of infected cells with a PKCα-specific shRNA (Fig. 8*A*) or antagonist (Fig. 8*B*) blocked vesicle formation, demonstrating a role for the kinase in their generation. DIC microscopy readily detected the vesicles in the absence of drug (Fig. 8 *A* and *B*, *Upper Right*), but failed to detect them when PKCα activity was reduced (Fig. 8 *A* and *B*, *Lower Right*), ruling out the possibility that vesicles accumulate lacking pUL99.

Vps34 Kinase Is Required to Generate the Large Vesicles and for Envelopment of Capsids. Vps34 phosphorylates phosphatidylinositol to generate PtdIns3*P*. The fact that EEA1 binds to PtdIns3*P* within endosomes (36) led us to explore the role of Vps34 during infection. As expected, shRNA-mediated knockdown of Vps34 (Fig. 9*A*, *Left*) reduced PtdIns3*P* levels in uninfected fibroblasts by a factor of 7–8 (Fig. 9*A*, *Right*). The knockdown eliminated accumulation of the large pUL99-positive vesicles in WT virus-infected cells (Fig. 9*B*, *Right*), whereas a nonspecific shRNA had no effect on the production of these vesicles (Fig. 9*B*, *Left*). Electron microscopy (Fig. 9*C*) showed that all cytoplasmic capsids observed in infected cells treated with a nonspecific shRNA were enveloped, whereas <1% of capsids were enveloped after treatment with Vps34-specific shRNA (Fig. 9*D*, *Left*). Knockdown of Vps34 did not significantly alter the number of

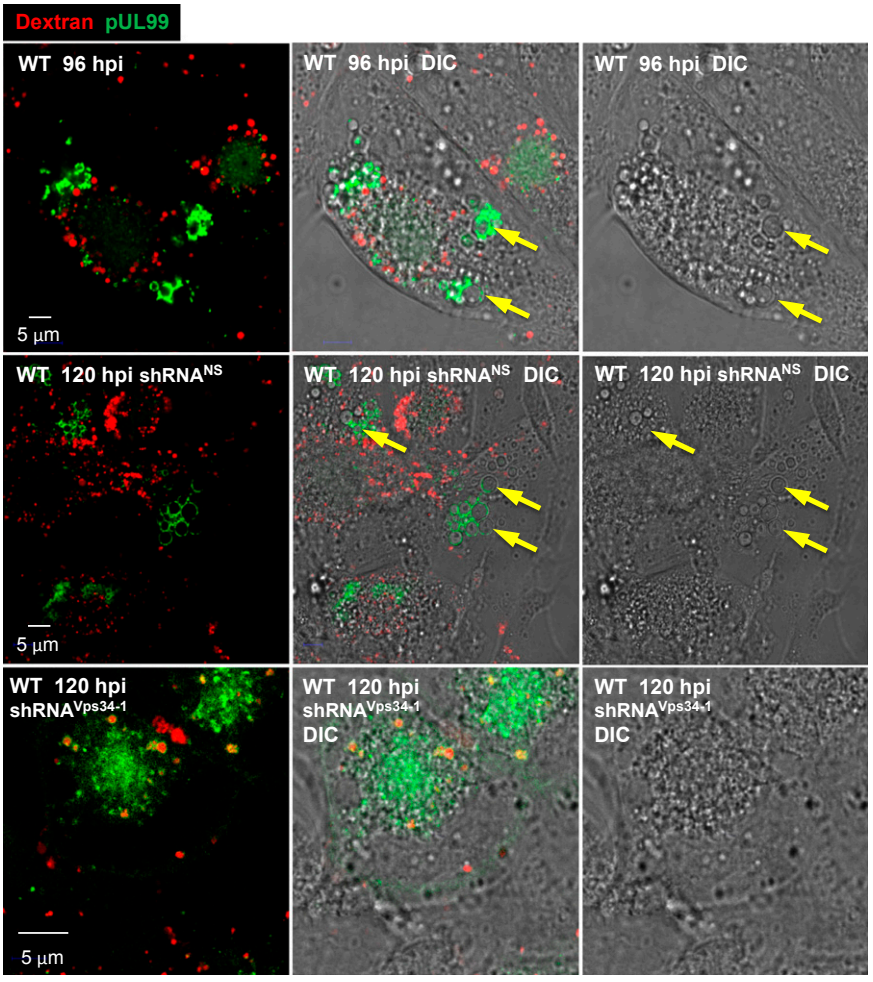

Fig. 7. Large infection-specific cytoplasmic vesicles do not exhibit early endosome activity. (*Top*) Fibroblasts were infected with WT HCMV and 96 h later treated with rhodamine-tagged dextran beads for 40 min at 37 °C, then assayed for the intracellular locations of the beads (red) and pUL99 (green). (*Middle* and *Bottom*) At 10 d after treatment with nonspecific or Vps34-specific shRNAs, fibroblasts were infected with WT virus at a multiplicity of 3 pfu/cell and assayed for the intracellular locations of the beads (red) and pUL99 (green). To confirm the presence of vesicles, cells were visualized by DIC microscopy as well. Examples of large infection-specific vesicles are indicated by arrows.

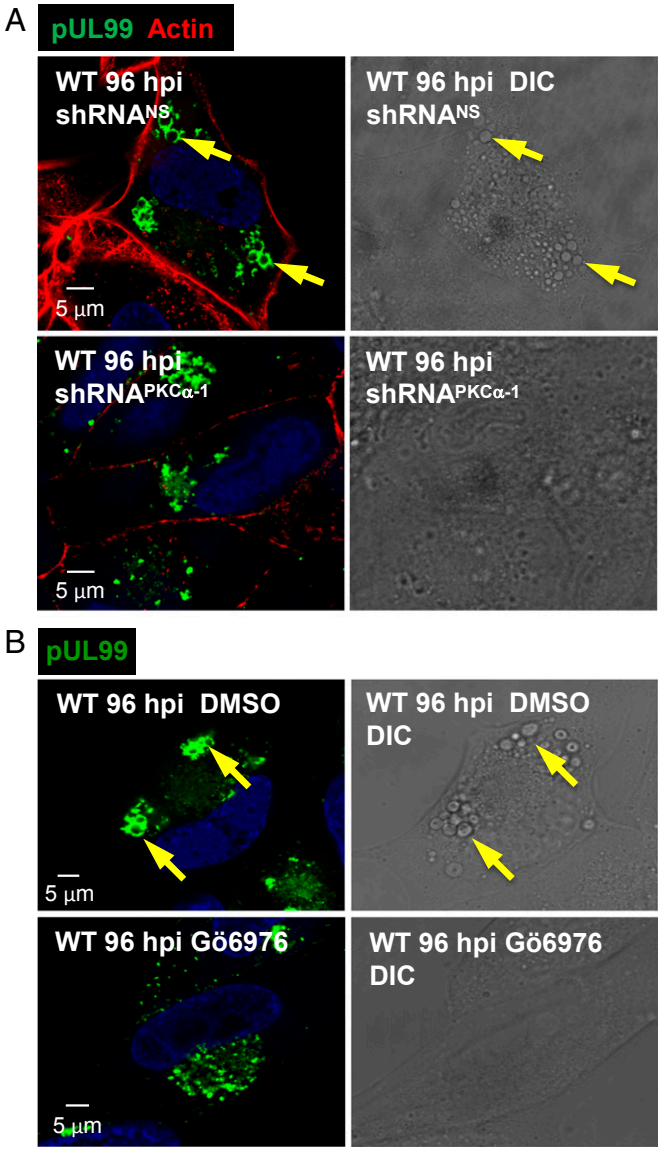

Fig. 8. PKCα is required for the production of large cytoplasmic vesicles after infection. (*A*) Knockdown of PKCα blocks production of large vesicles. Fibroblasts were treated with PKCα-specific shRNA or a nonspecific shRNA (NS), as described for Fig. 3. Cells were infected with WT virus and assayed by immunofluorescence for pUL99 (green) and actin (red) or by DIC microscopy at 96 hpi. (*B*) A PKCα antagonist blocks production of large vesicles. Fibroblasts were treated with solvent (DMSO) or 1 μM Gö6976 beginning 1 h after infection with WT virus. Cells received fresh medium with drug every 24 h, and were assayed by immunofluorescence for pUL99 (green) or by DIC microscopy at 96 hpi. Arrows indicate large vesicles identified in the immunofluorescent and DIC images of the same cell.

cytoplasmic capsids (Fig. 9*D*, *Center*), but the production of infectious virus was reduced by ≥1,000-fold (Fig. 9*D, Right*), consistent with the loss of enveloped capsids. Virus yield was also reduced by pharmacologic inhibition of Vps34 with 3-methyladenine.

As noted above, the C-terminal FYVE domain of EEA1 binds to the head group of PtdIns3*P* (35, 40). Transfection with a plasmid expressing a dimerized EEA1 FYVE domain (2xFYVE-GFP) (45) before infection blocked the production of pUL99-containing vesicles (Fig. 10*A*), presumably because 2xFYVE-GFP acted as a dominant negative protein, preventing the interaction of EEA1 with PtdIns3*P*. To confirm the relationship between de novo synthesis of PtdIns3*P* and the accumulation of the large pUL99-containing vesicles, we assayed for the presence of PtdIns3*P* in the vesicles using the GST-2xFYVE reporter (Fig. 10*B*). The vesicles contained PtdIns3*P*, as predicted by the presence of EEA1 (Fig. 6*A*) and their Vps34-dependent accumulation (Fig. 9*B*).

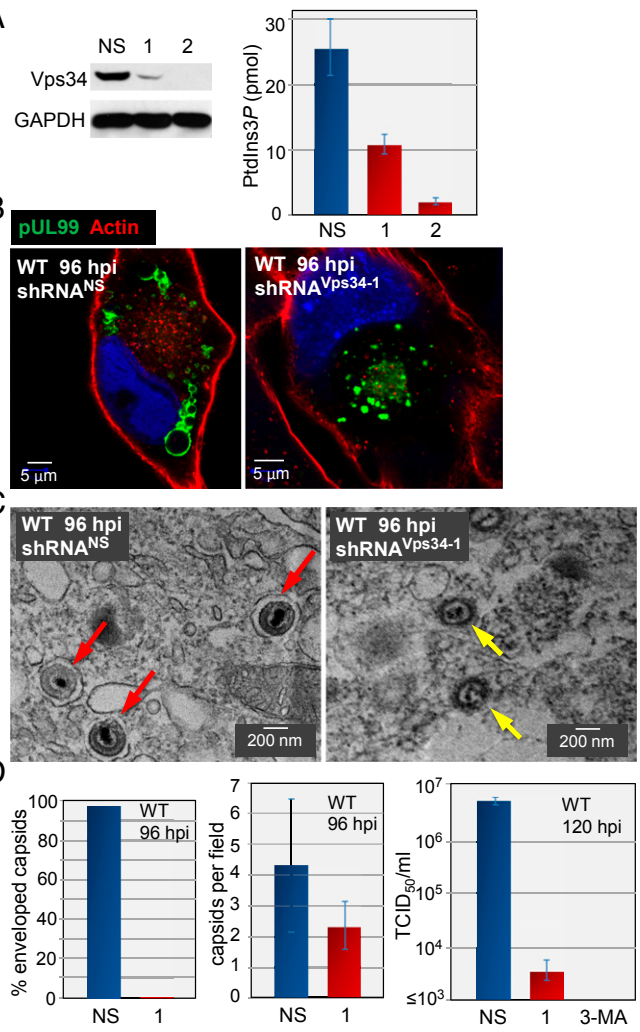

Fig. 9. Vps34 is required for the production of large cytoplasmic vesicles and enveloped HCMV progeny. (*A*) Vps34 is required for the production of vesicles. (*Left*) Fibroblasts were treated with nonspecific (NS) or Vps34-specific shRNAs (1 and 2) and 10 d later assayed by Western blot analysis using Vps34-specific antibody. GAPDH was assayed as a loading control. (*Right*) At 10 d after treatment with shRNAs, fibroblasts were assayed for PtdIns3*P* content. (*B*) At 10 d after treatment with shRNAs, fibroblasts were infected with WT HCMV and assayed for pUL99 (green) and actin (red). (*C*) Vps34 is required for the efficient production of infectious, enveloped virions. Representative electron micrographs are shown, with red arrows denoting enveloped particles and yellow arrows denoting capsids within cells treated with nonspecific or Vps34-specific shRNA after infection with WT virus. (*D*) Quantification of encapsidation and yield. (*Left*) A total of 200 cytoplasmic capsids were counted in nonspecific and Vps34-specific knockdown cells at 96 hpi with WT virus. (*Center*) Enveloped and nonenveloped capsids were counted in 50 fields, and the average ± SE numbers were determined. (*Right*) Fibroblasts treated with a nonspecific shRNA, Vps34-specific shRNA, or 5 mM 3-methyladenine (3-MA), added at 1 h after infection, were infected with WT HCMV, and extracellular virus yields were determined by plaque assay at 120 hpi.

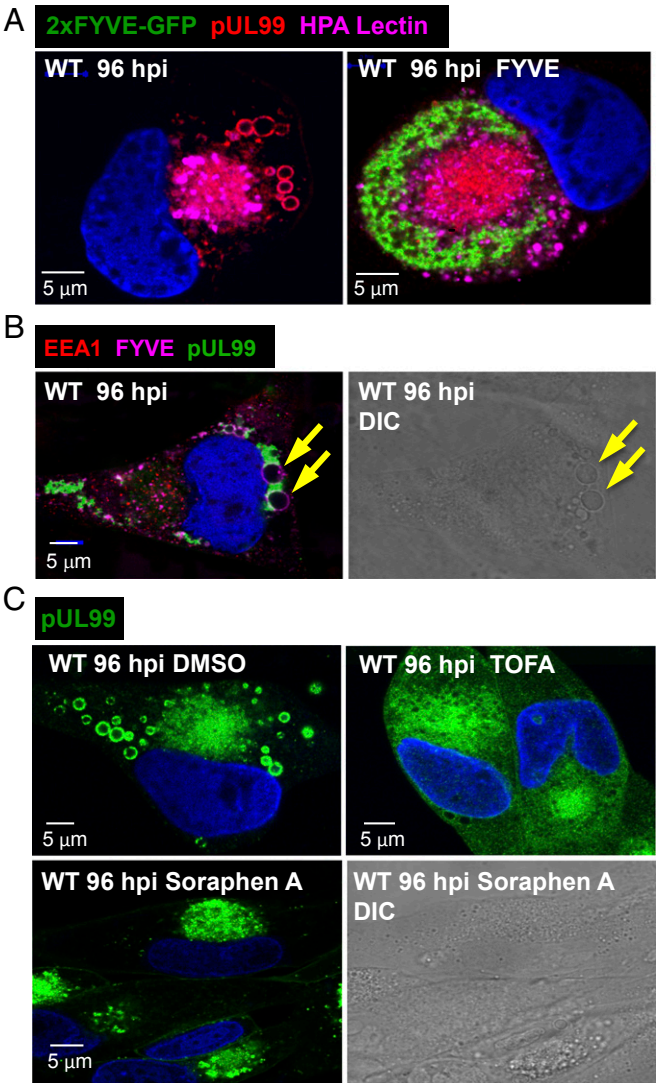

Fig. 10. Accumulation of large vesicles during the late phase of infection requires de novo fatty acid biosynthesis and PKCα activity. (*A*) A dimerized FYVE motif blocks production of infection-specific vesicles. Fibroblasts received no plasmid (*Left*) or received a plasmid expressing 2xFYVE-GFP (*Right*), and were infected 24 h later with WT virus. Cells were assayed at 96 hpi for 2xFYVE-GFP (green), pUL99 (red), and the Golgi tag, HPA lectin (purple). (*B*) Infection-specific vesicles contain PtdIns3*P*. WT-infected fibroblasts were assayed at 96 hpi for 2xFYVE-GFP binding (purple), pUL99 (green), and EEA1 (red). Arrows identify vesicles in the immunofluorescent and DIC images of the same cell. (*C*) Acetyl-CoA carboxylase inhibitors block the accumulation of infection-specific vesicles. Fibroblasts were treated with solvent (DMSO), 10 μg/mL TOFA, or 100 nM soraphen A starting at 1 h after infection with WT virus. Cells received fresh medium with drug every 24 h, and were assayed for pUL99 (green) or by DIC microscopy at 96 hpi.

To further probe the requirement for de novo synthesis of lipids to produce the vesicles, we treated infected cells with 5-tetradecyloxy-2-furoic acid (TOFA) (46). This drug inhibits acetyl-CoA carboxylase, blocking the production of malonylCoA, which is required by both fatty acid synthase and elongases to produce fatty acids. We have shown previously that this drug reduces the yield of HCMV by >1,000-fold (47), and here we found that it blocked the production of the large pUL99-positive vesicles as well (Fig. 10*C*, *Upper*). Soraphen A, a second acetyl-CoA carboxylase inhibitor (43), also blocked the production of large vesicles (Fig. 10*C*, *Lower Left*). DIC microscopy failed to detect the vesicles in the presence of soraphen A (Fig. 10*C*, *Lower Right*), ruling out the possibility that pUL99-deficient vesicles accumulate.

Discussion

Multiple lines of evidence demonstrate that PKCα is activated by pUL37x1 after HCMV infection of fibroblasts: (*i*) pUL37x1 induced the Ca^{2+}-dependent translocation of the kinase to the plasma membrane (Fig. 2), a hallmark of PKCα activation; (*ii*) the kinase resided in the DRM fraction after infection (Fig. 5*A*), consistent with earlier reports that activated PKCα interacts with caveolin-1 (26, 27), a constituent of lipid rafts (28, 29); and (*iii*) inhibition of PKCα activity reduced the yield of infectious virus (Fig. 3 *C* and *D*).

We have identified two consequences of PKCα activation. First, the kinase altered cell shape. Both PKCα activity (Fig. 3 *A* and *B*) and ROCK activity (Fig. 4 *A* and *B*) were required to induce cell rounding at 24 hpi. Only PKCα was critical for the efficient production of progeny virus (Figs. 3 *C* and *D* and 4*C*), arguing that cell rounding is not required for optimal virus replication. Second, PKCα (Fig. 8) and de novo lipid synthesis (Figs. 9*B* and 10*C*) were required for the accumulation of large vesicles within infected cells, and their appearance correlated with the efficient envelopment of capsids to produce infectious progeny (Fig. 9 *C* and *D*). These vesicles link earlier observations showing a requirement for de novo lipid synthesis to produce HCMV progeny (47, 48) with a specific morphological change in infected cells.

The effect of pUL37x1 on cell shape was confirmed by analysis of 3D reconstructions of cells loaded with a fluorescent dye, showing that fibroblasts undergo dynamic Ca^{2+}-dependent morphological changes as infection proceeds (Fig. 1). Uninfected fibroblasts were elongated and flat. By 24 hpi, the cells were spherical, and by 72 hpi, they converted to a more elongated, hemispherical shape. The dynamic changes in shape might result from a transient effect of Ca^{2+} mobilization; that is, the bulk of stored Ca^{2+} might be released to the cytosol and activate PKCα and ROCK signaling when pUL37x1 first accumulates. Alternatively, the virus or cell might modulate Ca^{2+}-signaling pathways as the infection proceeds, driving changes in shape. For example, μ-calpain–mediated cleavage (Fig. 5) might generate constitutive PKCα activity (14, 34). The inhibition of p53 transcriptional activity by HCMV (49, 50) also could contribute to the change in shape, because p53-deficient mouse fibroblasts cultured in 3D matrices undergo a ROCK-dependent transition from an elongated to spherical morphology (24). One consequence of p53 loss is increased cell movement, which could support the spread of HCMV within an infected host. Indeed, the levels of many cell-surface adhesion molecules change after infection (51), and the altered shape could result from multiple changes that promote detachment of infected cells from their substrates. Thus, altered cell shape might contribute to the spread of virus within an infected host via cell motility rather than mediating a cell-autonomous effect on virus yield.

Additional morphological changes besides altered cell shape were noted after infection with HCMV (6). The nucleus was enlarged and assumed a kidney shape, the viral AC was formed, and large cytoplasmic vesicles accumulated (Fig. 6 *A* and *B*). The vesicles, which have been reported previously (7, 39), ranged in diameter from approximately 0.5 μM to nearly 5 μM. They appeared late during the infection cycle, and the EEA1 early endosome marker and pUL99 virion protein localized at their periphery. The large vesicles did not accumulate after infection with a pUL37x1-deficient virus, when the AC was visualized by staining with multiple markers (Fig. 6*A*).

How does pUL37x1 control formation of the large vesicles? PKCα activity induced by the viral protein (Fig. 2 and Fig. 5*A*) is required (Fig. 8). However, although the kinase can localize to early and late endosomes (52) as well as recycling endosomes

(53), how the enzyme supports formation of the large vesicles is unclear. Their production also requires de novo fatty acid (Fig. 10*C*) and PtdIns3*P* biosynthesis (Fig. 9*B*), leading us to speculate that pUL37x1 is acting to facilitate their genesis in part through a second Ca^{2+}-dependent kinase, calmodulin kinase kinase (CaMKK). CaMKK has been shown to be required for HCMV-induced activation of glycolysis and efficient production of virus progeny (54), and it could be activated by pUL37x1-induced release of Ca^{2+} stores into the cytosol. Because elevated flux through central carbon metabolism leads to increased efflux of carbon to the fatty acid biosynthetic pathway in HCMV-infected cells (47), pUL37x1-mediated activation of CaMKK might facilitate the de novo lipid synthesis required for production of the large vesicles.

Although the vesicles contain PtdIns3*P* and EEA1 (Fig. 10*B*), markers of early endosomes (35, 36), they did not accumulate dextran from the medium (Fig. 7), as would have been expected for functional early endosomes (43). The vesicles could be byproducts of elevated lipid synthesis. Newly synthesized lipids might initially contribute to membrane formation within the AC, and the large vesicles might subsequently arise from fusion of AC membranes during the late phase of infection. As a result, they could be functionally inert or redundant with smaller vesicles located in the AC. If this were the case, then pUL37x1 might modify the AC to facilitate the envelopment of capsids. Alternatively, because inhibition of large vesicle formation by abrogation of Vps34 activity (Fig. 9*B*) was correlated with reduced envelopment of capsids and reduced production of progeny virus (Fig. 9 *C* and *D*), it is conceivable that HCMV capsids also mature at the large vesicles; that is, envelopment might occur both within the AC and at the large vesicles.

HCMV pUL37x1 causes the release of Ca^{2+} stores, initiating a cascade of events required for the efficient production of viral progeny. The identification of PKCα as a key element of this cascade provides a framework for further dissection of the complex interplay between signal transduction and morphological alterations after HCMV infection.

Methods

Viruses, Cells, Plasmids, and Drugs. WT HCMV strain AD169 (BAD*wt*) and a pUL37x1-deficient derivative (BAD*sub*UL37x1) have been described previously (10, 55). HCMV was propagated in primary human foreskin fibroblasts maintained in DMEM containing 10% FCS. Infectious HCMV was quantified by a tissue culture infectious dose 50 ($TCID_{50}$) assay on fibroblasts, and all infections were performed at a multiplicity of 5 pfu/cell unless specified otherwise.

Plasmids expressing pUL37x1-GFP (a gift from A. Watson, Children's National Medical Center, Washington, DC) (10), PKCα-GFP (a gift from C. Larsson, Lund University, Lund, Sweden) (16), and 2xFYVE-GFP (a gift from H. Stenmark, Oslo University Hospital, Oslo, Norway) (56) have been described previously. The PKCα inhibitor Gö6976 (Sigma-Aldrich) (57), ROCK inhibitors Y27632 (Enzo Life Sciences) (58) and GSK429286A (Selleckchem) (59), acetyl-CoA carboxylase inhibitors 5-tetradecyloxy-2-furoic acid (TOFA; Cayman) (46) and soraphen A (a gift from Kadmon Pharmaceuticals) (60), and 3-methyladenine (Sigma-Aldrich) (61) were prepared in DMSO and diluted into cell culture medium at the indicated final concentrations. Cultures received fresh drug-containing medium every 24 h.

Immunofluorescence Assays. Indirect immunofluorescence was performed using antibodies to HCMV pUL37x1 (10), HCMV pUL99 (62), HCMV IE1 (63), EEA1 (Enzo Life Sciences), and vinculin (Sigma-Aldrich), together with Alexa Fluor 568-conjugated anti-mouse secondary antibody (Invitrogen). Actin was detected with Alexa Fluor 488 phalloidin (Invitrogen), and the Golgi tag Alexa Fluor 488-conjugated lectin HPA (Life Technologies) served as a marker for the HCMV AC. Nuclear DNA was stained with DAPI (Invitrogen). Fluorescent and DIC images were captured with a Leica SP5 confocal microscope, and images were analyzed with Volocity 3D image analysis software (Perkin-Elmer).

To monitor cell shape and volume, 5 μM calcein green AM or calcein red-orange AM (Invitrogen) was added to culture medium, and cells were incubated for 30 min at 37 °C. Single live cells were examined by confocal laser scanning fluorescence microscopy (Perkin-Elmer Ultraview RS-3), image stacks were rendered into 3D images, and cell volumes were determined using Volocity 3D image analysis software.

To monitor endocytosis, cells were incubated with 3 mg/mL rhodamine B-labeled dextran (10 kDa; Life Technologies) for 10 min at 37 °C, washed, and then refed with dextran-free medium. After incubation at 37 °C, internalized dextran was observed by fluorescence microscopy.

Knockdown of Cellular Protein Expression. Knockdown experiments used shRNAs (Sigma-Aldrich) with the following target sequences: PKCα shRNA1, 5′-CCGGCTTTGGAGTTTCGGAGCTGATCTCGAGATCAGCTCCGAAACTCCAAAGTTTTT-3′; PKCα shRNA2, 5′-CCGGCGAGCTATTTCAGTCTATCATCTCGAGATGATAGACTGAAATAGCTCGTTTTT-3′; PKCα shRNA3, 5′-CCGGCATGGAACTCAGGCAGAAATTCTCGAGAATTTCTGCCTGAGTTCCATGTTTTT-3′; μ-calpain shRNA1, 5′-CCGGAGAGGAGATTGACGAGAACTTCTCGAGAAGTTCTCGTCAATCTCCTCTTTTTT-3′; μ-calpain shRNA2, 5′-CCGGCGACATGGAGACTATTGGCTTCTCGAGAAGCCAATAGTCTCCATGTCGTTTTT-3′; Vps34 shRNA1, 5′-CCGGCCACGAGAGATCAGTTAAATACTCGAGTATTTAACTGATCTCTCGTGG TTTTTG-3′; Vps34 shRNA2, 5′-CCGGCCAAGTGAGAATGGGCCAAATCTCGAGATTTGGCCCATTCTCACTTGGTTTTTG-3′; nonspecific shRNA, 5′-CAACAAGATGAAGAGCACCAATTCAAGAGATTGGTGCTCTTCATCTTGTTGTTTTTTGT-3′.

Vectors (pLKO.1-puro) expressing shRNAs were packaged, and fibroblasts were transduced with vectors on three consecutive days, selected using 3 μg/mL puromycin, and then used for HCMV infection.

Lipid Raft/DRM Assay. Lipid rafts were analyzed using Optiprep sucrose gradients (64). Approximately 10^7 fibroblasts were harvested by scraping, washed twice with culture medium, and lysed at 4 °C in 1 mL of lysis buffer (1% Triton X-100, 25 mM Tris·HCl pH 6.8, 150 mM NaCl, 5 mM EDTA, 5 mM iodoacetamide, and protease inhibitor mixture; Roche Diagnostics). The lysate was passed 15 times through an 18-gauge needle, rocked in a tube for 30 min at 4 °C, passed again through the needle, and then mixed with 2 mL of 4 °C Optiprep (Sigma-Aldrich). A 3-mL sample was placed into an SW41 ultracentrifuge tube, overlaid with 5 mL of 4 °C 30% (vol/vol) Optiprep followed by 4 mL of 5% (vol/vol) Optiprep, both in 25 mM Tris·HCl pH 6.8, 150 mM NaCl, and 5 mM EDTA. Samples were centrifuged at 200,000 × *g* at 4 °C for 20 h. Fractions was analyzed by Western blot assay using antibodies to transferrin receptor (Zymed), EEA1 (Enzo Life Sciences), PKCα, and μ-calpain (Cell Signaling). Ganglioside GM1 was assayed using biotinylated cholera toxin B subunit (Sigma-Aldrich).

PtdIns3*P* Staining and Quantification. Endogenous PtdIns3*P* was detected using a biotinylated-GST:2xFYVE probe. The 2xFYVE domain from a GFP:2xFYVE construct (56) was excised and ligated into pGEX-2T. Control GST and GST-2xFYVE were purified using glutathione resin (Clontech), followed by anion-exchange chromatography with Source 15Q medium (GE Healthcare). Proteins were then biotinylated with Sulfo-NHS-LC-Biotin (Pierce). Free biotin was separated from biotinylated protein via two sequential runs on a HiTrap desalting column (GE Healthcare), and fractions containing the biotinylated probe were pooled and stored at −80 °C. To visualize FYVE binding domains, fibroblasts were washed twice with PBS, fixed with 4% paraformaldehyde in PBS for 12 h, and then permeabilized with 0.05% saponin (Sigma-Aldrich) in PBS for 10 min. Cells were then washed with PBS and quenched with 60 mM NH_4Cl_2, blocked with 5% BSA in PBS for 1 h, and incubated with 40 μg/mL biotin-GST:2xFYVE in PBS containing 2% BSA for 1 h, all at room temperature. Cells were then washed with 2% BSA in PBS and incubated with 1:1,000 streptavidin-Alexa Fluor 647 (Life Technologies) in PBS with 2% BSA for 1 h. Nuclei were stained with 1 μg/mL Hoechst 33342 (Life Technologies).

PtdIns3*P* was quantified by competitive ELISA (Echelon Biosciences) in which experimental samples were matched to a standard curve generated by simultaneous readings of known amounts of PtdIns3*P*.

ACKNOWLEDGMENTS. We thank A. Oberstein (Princeton) for the GST-2xFYVE expression vector and advice on purification and biotinylation of the protein. We acknowledge the kind gifts of plasmids from A. Watson (Children's National Medical Center) and C. Larsson (Lund University), and the generous gift of soraphen A from Kadmon Pharmaceuticals. This work was supported by National Institutes of Health Grants CA82396 and AI078063.

1. Britt W (2008) Manifestations of human cytomegalovirus infection: Proposed mechanisms of acute and chronic disease. *Curr Top Microbiol Immunol* 325:417–470.

2. Dziurzynski K, et al.; HCMV and Gliomas Symposium (2012) Consensus on the role of human cytomegalovirus in glioblastoma. *Neuro-oncol* 14(3):246–255.

3. Streblow DN, Dumortier J, Moses AV, Orloff SL, Nelson JA (2008) Mechanisms of cytomegalovirus-accelerated vascular disease: Induction of paracrine factors that promote angiogenesis and wound healing. *Curr Top Microbiol Immunol* 325: 397–415.
4. Moss P (2010) The emerging role of cytomegalovirus in driving immune senescence: A novel therapeutic opportunity for improving health in the elderly. *Curr Opin Immunol* 22(4):529–534.
5. Weller TH, Hanshaw JB, Scott DE (1960) Serologic differentiation of viruses responsible for cytomegalic inclusion disease. *Virology* 12:130–132.
6. Alwine JC (2012) The human cytomegalovirus assembly compartment: A masterpiece of viral manipulation of cellular processes that facilitates assembly and egress. *PLoS Pathog* 8(9):e1002878.
7. Sanchez V, Greis KD, Sztul E, Britt WJ (2000) Accumulation of virion tegument and envelope proteins in a stable cytoplasmic compartment during human cytomegalovirus replication: Characterization of a potential site of virus assembly. *J Virol* 74(2): 975–986.
8. Seo JY, Britt WJ (2007) Cytoplasmic envelopment of human cytomegalovirus requires the postlocalization function of tegument protein pp28 within the assembly compartment. *J Virol* 81(12):6536–6547.
9. Poncet D, et al. (2006) Cytopathic effects of the cytomegalovirus-encoded apoptosis inhibitory protein vMIA. *J Cell Biol* 174(7):985–996.
10. Sharon-Friling R, Goodhouse J, Colberg-Poley AM, Shenk T (2006) Human cytomegalovirus pUL37x1 induces the release of endoplasmic reticulum calcium stores. *Proc Natl Acad Sci USA* 103(50):19117–19122.
11. Williamson CD, Colberg-Poley AM (2009) Access of viral proteins to mitochondria via mitochondria-associated membranes. *Rev Med Virol* 19(3):147–164.
12. McCormick AL (2008) Control of apoptosis by human cytomegalovirus. *Curr Top Microbiol Immunol* 325:281–295.
13. Holinstat M, Mehta D, Kozasa T, Minshall RD, Malik AB (2003) Protein kinase C alpha-induced p115RhoGEF phosphorylation signals endothelial cytoskeletal rearrangement. *J Biol Chem* 278(31):28793–28798.
14. Young S, Parker PJ, Ullrich A, Stabel S (1987) Down-regulation of protein kinase C is due to an increased rate of degradation. *Biochem J* 244(3):775–779.
15. Newton AC (2010) Protein kinase C: Poised to signal. *Am J Physiol Endocrinol Metab* 298(3):E395–E402.
16. Raghunath A, Ling M, Larsson C (2003) The catalytic domain limits the translocation of protein kinase C alpha in response to increases in Ca^{2+} and diacylglycerol. *Biochem J* 370(Pt 3):901–912.
17. Svensson K, Zeidman R, Trollér U, Schultz A, Larsson C (2000) Protein kinase C beta1 is implicated in the regulation of neuroblastoma cell growth and proliferation. *Cell Growth Differ* 11(12):641–648.
18. Stanton RJ, et al. (2007) Cytomegalovirus destruction of focal adhesions revealed in a high-throughput Western blot analysis of cellular protein expression. *J Virol* 81(15): 7860–7872.
19. Peng X, Nelson ES, Maiers JL, DeMali KA (2011) New insights into vinculin function and regulation. *Int Rev Cell Mol Biol* 287:191–231.
20. Dovas A, et al. (2010) Serine 34 phosphorylation of rho guanine dissociation inhibitor (RhoGDIalpha) links signaling from conventional protein kinase C to RhoGTPase in cell adhesion. *J Biol Chem* 285(30):23296–23308.
21. Dwyer LD, Miller AC, Parks AL, Jaken S, Malkinson AM (1994) Calpain-induced down-regulation of activated protein kinase C-alpha affects lung epithelial cell morphology. *Am J Physiol* 266(5 Pt 1):L569–L576.
22. Slater SJ, Seiz JL, Stagliano BA, Stubbs CD (2001) Interaction of protein kinase C isozymes with Rho GTPases. *Biochemistry* 40(14):4437–4445.
23. Riento K, Ridley AJ (2003) Rocks: Multifunctional kinases in cell behaviour. *Nat Rev Mol Cell Biol* 4(6):446–456.
24. Gadea G, de Toledo M, Anguille C, Roux P (2007) Loss of p53 promotes RhoA-ROCK–dependent cell migration and invasion in 3D matrices. *J Cell Biol* 178(1): 23–30.
25. Petroll WM, Ma L, Kim A, Ly L, Vishwanath M (2008) Dynamic assessment of fibroblast mechanical activity during Rac-induced cell spreading in 3-D culture. *J Cell Physiol* 217 (1):162–171.
26. Oka N, et al. (1997) Caveolin interaction with protein kinase C: Isoenzyme-dependent regulation of kinase activity by the caveolin scaffolding domain peptide. *J Biol Chem* 272(52):33416–33421.
27. Stubbs CD, Botchway SW, Slater SJ, Parker AW (2005) The use of time-resolved fluorescence imaging in the study of protein kinase C localisation in cells. *BMC Cell Biol* 6(1):22.
28. Al Z, Cohen CM (1993) Phorbol 12-myristate 13-acetate–stimulated phosphorylation of erythrocyte membrane skeletal proteins is blocked by calpain inhibitors: Possible role of protein kinase M. *Biochem J* 296(Pt 3):675–683.
29. Verkade P, Simons K (1997) Robert Feulgen Lecture 1997: Lipid microdomains and membrane trafficking in mammalian cells. *Histochem Cell Biol* 108(3):211–220.
30. Simons K, Gerl MJ (2010) Revitalizing membrane rafts: New tools and insights. *Nat Rev Mol Cell Biol* 11(10):688–699.
31. Goswami D, et al. (2008) Nanoclusters of GPI-anchored proteins are formed by cortical actin-driven activity. *Cell* 135(6):1085–1097.
32. Viola A, Gupta N (2007) Tether and trap: Regulation of membrane-raft dynamics by actin-binding proteins. *Nat Rev Immunol* 7(11):889–896.
33. Kishimoto A, et al. (1989) Limited proteolysis of protein kinase C subspecies by calcium-dependent neutral protease (calpain). *J Biol Chem* 264(7):4088–4092.
34. Tapley PM, Murray AW (1984) Modulation of Ca^{2+}-activated, phospholipid-dependent protein kinase in platelets treated with a tumor-promoting phorbol ester. *Biochem Biophys Res Commun* 122(1):158–164.
35. Simonsen A, et al. (1998) EEA1 links PI(3)K function to Rab5 regulation of endosome fusion. *Nature* 394(6692):494–498.
36. Mu FT, et al. (1995) EEA1 is a conserved alpha-helical peripheral membrane protein flanked by cysteine "fingers" and contains a calmodulin-binding IQ motif. *J Biol Chem* 270(22):13503–13511.
37. Cepeda V, Esteban M, Fraile-Ramos A (2010) Human cytomegalovirus final envelopment on membranes containing both trans-Golgi network and endosomal markers. *Cell Microbiol* 12(3):386–404.
38. Das S, Pellett PE (2011) Spatial relationships between markers for secretory and endosomal machinery in human cytomegalovirus-infected cells versus those in uninfected cells. *J Virol* 85(12):5864–5879.
39. Seo JY, Britt WJ (2008) Multimerization of tegument protein pp28 within the assembly compartment is required for cytoplasmic envelopment of human cytomegalovirus. *J Virol* 82(13):6272–6287.
40. Jovic M, Sharma M, Rahajeng J, Caplan S (2010) The early endosome: A busy sorting station for proteins at the crossroads. *Histol Histopathol* 25(1):99–112.
41. Sanchez V, Sztul E, Britt WJ (2000) Human cytomegalovirus pp28 (UL99) localizes to a cytoplasmic compartment which overlaps the endoplasmic reticulum-golgi-intermediate compartment. *J Virol* 74(8):3842–3851.
42. Nazarewicz RR, et al. (2011) Early endosomal antigen 1 (EEA1) is an obligate scaffold for angiotensin II-induced, PKC-alpha-dependent Akt activation in endosomes. *J Biol Chem* 286(4):2886–2895.
43. Morel E, Gruenberg J (2007) The p11/S100A10 light chain of annexin A2 is dispensable for annexin A2 association to endosomes and functions in endosomal transport. *PLoS ONE* 2(10):e1118.
44. Johnson EE, Overmeyer JH, Gunning WT, Maltese WA (2006) Gene silencing reveals a specific function of hVps34 phosphatidylinositol 3-kinase in late versus early endosomes. *J Cell Sci* 119(Pt 7):1219–1232.
45. Gillooly DJ, Raiborg C, Stenmark H (2003) Phosphatidylinositol 3-phosphate is found in microdomains of early endosomes. *Histochem Cell Biol* 120(6):445–453.
46. Kariya T, Wille LJ (1978) Inhibition of fatty acid synthesis by RMI 14,514 (5-tetradecyloxy-2-furoic acid). *Biochem Biophys Res Commun* 80(4):1022–1024.
47. Munger J, et al. (2008) Systems-level metabolic flux profiling identifies fatty acid synthesis as a target for antiviral therapy. *Nat Biotechnol* 26(10):1179–1186.
48. Koyuncu E, Purdy JG, Rabinowitz JD, Shenk T (2013) Saturated very long chain fatty acids are required for the production of infectious human cytomegalovirus progeny. *PLoS Pathog* 9(5):e1003333.
49. Jault FM, et al. (1995) Cytomegalovirus infection induces high levels of cyclins, phosphorylated Rb, and p53, leading to cell cycle arrest. *J Virol* 69(11):6697–6704.
50. Savaryn JP, et al. (2013) Human cytomegalovirus pUL29/28 and pUL38 repression of p53-regulated p21CIP1 and caspase 1 promoters during infection. *J Virol* 87(5): 2463–2474.
51. Gudleski-O'Regan N, Greco TM, Cristea IM, Shenk T (2012) Increased expression of LDL receptor-related protein 1 during human cytomegalovirus infection reduces virion cholesterol and infectivity. *Cell Host Microbe* 12(1):86–96.
52. Lum MA, Pundt KE, Paluch BE, Black AR, Black JD (2013) Agonist-induced down-regulation of endogenous protein kinase c α through an endolysosomal mechanism. *J Biol Chem* 288(18):13093–13109.
53. Becker KP, Hannun YA (2003) cPKC-dependent sequestration of membrane-recycling components in a subset of recycling endosomes. *J Biol Chem* 278(52):52747–52754.
54. McArdle J, Schafer XL, Munger J (2011) Inhibition of calmodulin-dependent kinase kinase blocks human cytomegalovirus-induced glycolytic activation and severely attenuates production of viral progeny. *J Virol* 85(2):705–714.
55. Yu D, Smith GA, Enquist LW, Shenk T (2002) Construction of a self-excisable bacterial artificial chromosome containing the human cytomegalovirus genome and mutagenesis of the diploid TRL/IRL13 gene. *J Virol* 76(5):2316–2328.
56. Gillooly DJ, et al. (2000) Localization of phosphatidylinositol 3-phosphate in yeast and mammalian cells. *EMBO J* 19(17):4577–4588.
57. Martiny-Baron G, et al. (1993) Selective inhibition of protein kinase C isozymes by the indolocarbazole Gö 6976. *J Biol Chem* 268(13):9194–9197.
58. Uehata M, et al. (1997) Calcium sensitization of smooth muscle mediated by a Rho-associated protein kinase in hypertension. *Nature* 389(6654):990–994.
59. Goodman KB, et al. (2007) Development of dihydropyridone indazole amides as selective Rho-kinase inhibitors. *J Med Chem* 50(1):6–9.
60. Vahlensieck HF, Pridzun L, Reichenbach H, Hinnen A (1994) Identification of the yeast ACC1 gene product (acetyl-CoA carboxylase) as the target of the polyketide fungicide soraphen A. *Curr Genet* 25(2):95–100.
61. Miller S, Oleksy A, Perisic O, Williams RL (2010) Finding a fitting shoe for Cinderella: Searching for an autophagy inhibitor. *Autophagy* 6(6):805–807.
62. Silva MC, Yu QC, Enquist L, Shenk T (2003) Human cytomegalovirus UL99-encoded pp28 is required for the cytoplasmic envelopment of tegument-associated capsids. *J Virol* 77(19):10594–10605.
63. Zhu H, Shen Y, Shenk T (1995) Human cytomegalovirus IE1 and IE2 proteins block apoptosis. *J Virol* 69(12):7960–7970.
64. Lyman MG, Curanovic D, Enquist LW (2008) Targeting of pseudorabies virus structural proteins to axons requires association of the viral Us9 protein with lipid rafts. *PLoS Pathog* 4(5):e1000065.